

An End-to-End Network for Co-Saliency Detection in One Single Image

Yuanhao Yue¹, Qin Zou^{1*}, Hongkai Yu², Qian Wang¹, Song Wang³

¹School of Computer Science, Wuhan University, China

²Department of Computer Science, University of Texas - Rio Grande Valley, USA

³Department of Computer Science and Engineering, University of South Carolina, USA

Abstract

As a common visual problem, co-saliency detection within a single image does not attract enough attention and yet has not been well addressed. Existing methods often follow a bottom-up strategy to infer co-saliency in an image, where salient regions are firstly detected using visual primitives such as color and shape, and then grouped and merged into a co-saliency map. However, co-saliency is intrinsically perceived in a complex manner with bottom-up and top-down strategies combined in human vision. To deal with this problem, a novel end-to-end trainable network is proposed in this paper, which includes a backbone net and two branch nets. The backbone net uses ground-truth masks as top-down guidance for saliency prediction, while the two branch nets construct triplet proposals for feature organization and clustering, which drives the network to be sensitive to co-salient regions in a bottom-up way. To evaluate the proposed method, we construct a new dataset of 2,019 nature images with co-saliency in each image. Experimental results show that the proposed method achieves a state-of-the-art accuracy with a running speed of 28fps.

Introduction

In the past two decades, saliency detection (Hou and Zhang 2007; Goferman *et al.* 2011; Cheng *et al.* 2014) has attracted wide attention from the vision community. However, most existing methods define the problem as cross-image co-saliency detection (Fu *et al.* 2013; Cao *et al.* 2014; Huang *et al.* 2017), which highlights the objects co-occurring in multiple images, e.g., a pair of images or a video sequence (Wei *et al.* 2017; Wang *et al.* 2018). While cross-image co-saliency detection has been extensively studied, another co-saliency detection problem - within-image co-saliency detection (Yu *et al.* 2018) - has not been well addressed yet.

Within-image co-saliency detection aims at highlighting multiple occurrences of a same object class with similar appearance in a single image. For human vision, this is a common visual ability and has been frequently used in our daily life, e.g, spotting the players of the same team in the sports field, counting the beans in the plat, etc. However, for computer vision, it is still a challenge to ask the algorithm itself

*Corresponding Author: Qin Zou (qzou@whu.edu.cn).

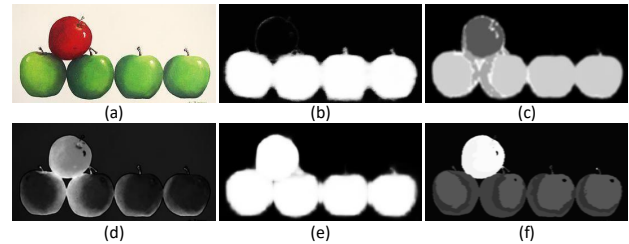


Figure 1: An illustration of within-image co-saliency detection. The top row shows: (a) an input image containing four green apples and one red apple, (b) co-saliency map obtained by the proposed method, and (c) the result produced by Yu *et al.* (2018). The bottom row shows the results obtained by three general saliency detection methods without considering the co-occurrence of a same object class.

to find proposal groups which include co-occurring saliency regions in a single image. Until now, only a few researches give direct consideration on this problem.

The pioneering research in Yu *et al.* (2018) presented a two-stage method for within-image co-saliency detection. The first stage generates object proposals using the classical EdgeBox (Zitnick and Dollár 2014), and the second stage computes co-saliency by deriving proposal groups with good common saliency, based on mutual similarity scores. This typical bottom-up strategy often suffers from high computation cost in processing low-level features and low integrity in constructing a unified optimization model for co-saliency learning, i.e., cannot work in an end-to-end manner.

Some other typical works such as RFCN (Wang *et al.* 2016), DCL (Li and Yu 2016) and CPF (Zhao and Wu 2019) learn high level features for salient object detection using deep neural networks, which directly use human-annotated saliency masks to guide the training in a top-down manner. However, co-saliency is intrinsically perceived in a complex manner by combining bottom-up and top-down strategies. Solely using one of these strategies would not obtain satisfactory results. An example is shown in Figure 1, in which the top three results are obtained by the general

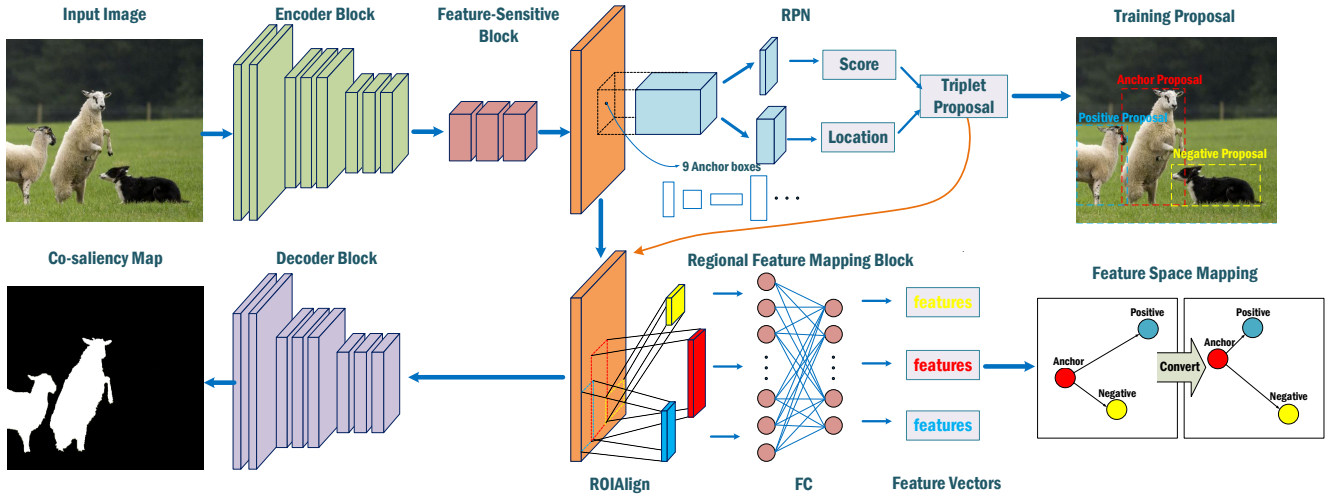


Figure 2: The schematic illustration of our network. The encoder and decoder blocks adopt the the skip-layer structures within the U-net architecture. Feature-Sensitive block is composed of three trainable 3×3 convolution layers. In the training phase, Feature-Sensitive block is supervised by two kinds of supervisory signals, i.e., Region Proposal Network (RPN) and Regional Feature Mapping (RFM). RPN regresses the confidences and locations of saliency regions and provides training samples for the Regional Feature Mapping Block (RFM). The RFM network transforms the corresponding region features to feature vectors with a fixed length.

saliency detection methods.

Based on the discussion above, we study to combine the top-down and bottom-up strategies together, and propose an end-to-end trainable deep neural network for within-image co-saliency detection. When using high-level features for common saliency object identification, the key point is how to make high-level layers be sensitive to the co-saliency regions. We employ an encoder-decoder architecture as the backbone net for co-saliency map prediction, and two branch nets to guide the training process and make the learned model more sensitive to co-salient regions. One branch net is a region proposal network (Ren *et al.* 2015) (RPN), producing triplet proposals. The other branch net is a regional feature mapping (RFM), which works in a bottom-up manner to drive the backbone net to be sensitive to co-salient regions. Triplet feature similarity is considered to construct the training loss (Schroff *et al.* 2015; Bell and Bala 2015).

The whole network is trained in a simple data-driven manner, thereby avoiding complex fusion strategies, improving the speed and making the training simple and effective. Once the training is done, the backbone net is used to make an end-to-end prediction of co-saliency map for an input image. It achieves the state-of-the-art accuracy on two targeted datasets and runs in a speed much faster than the competing methods. The main contributions of this work lie in three-fold:

- First, a unified end-to-end network is proposed for co-saliency detection in a single image. It combines the top-down and bottom-up strategies: a backbone net, i.e., encoder-decoder net, is used for co-saliency map prediction, and two branch nets, i.e., RPN and RFM, are used to

drive the network to be sensitive to co-salient regions.

- Second, an online training sample selection strategy is presented. It enhances the proposed method in helping it obtain much higher accuracy than the offline selection strategy with random scaling and offset.
- Third, a new dataset for within-image saliency detection is constructed. It contains 2,019 nature images of more than 300 classes, with instance-level annotations. The dataset, as well as the codes and trained models, will be released to the public, which can be used as a benchmark and would promote the research in this field.

Proposed Approach

Problem Formulation

Within-image co-saliency detection aims at discovering the common and salient objects with similar appearance in a single image. If two or more detected objects show high-level of similarity and belong to the same object, this category area will be highlighted in the resulting co-saliency map. We simplified the experimental scenario by removing images that did not contain objects of the same category. Given a training data set containing N images as $S = \{(X^n, Y^n), n = 1, \dots, N\}$, where $X^n = \{x_i^{(n)}, i = 1, \dots, I\}$ denotes the raw image, $Y^n = \{y_i^{(n)}, i = 1, \dots, I, y_i^{(n)} \in \{0, 1\}\}$ denotes the binary image of the regions containing saliency objects of the same class, I denotes the number of pixel in image, the goal of the co-saliency detection model $F(\cdot)$ is to train the network to produce prediction salient maps $P = \{p_i^{(n)}, n = 1, \dots, N\}$

approaching the ground truth annotated by experts:

$$P = F(X; \Theta), \quad (1)$$

where Θ represents optimized model parameters in this work.

Methodology

The model is divided into four main parts, as shown in Figure 2. First, the original image is input into the pre-trained feature extraction network, i.e., the encoder block, to generate high-level semantic feature maps. Then, the feature maps are fed into the Feature-Sensitive block to extract the feature map that is sensitive to the co-saliency regions in the image. In the training phase, the Feature-Sensitive block is supervised by two kinds of supervisory signals, one from the decoder block and the other from the regional feature mapping network (RFM). Among them, the decoder block outputs the corresponding final saliency map, while RFM network outputs the high-level feature coding and position regression of the salient object region corresponding to the original input image. In the evaluation phase, co-saliency regions are predicted only through the encoder-decoder backbone net and the Feature-Sensitive block.

Encoder-Decoder Block The encoder and decoder blocks in our network are based on U-Net (Ronneberger *et al.* 2015). The encoder and decoder blocks adopt the skip-layer structures. The encoder block adopts the convolution part of pre-trained VGG-16 network (Simonyan and Zisserman 2014) targeted on the classification task on the ImageNet dataset (Deng *et al.* 2009). Its parameters are frozen and thus will not participate in the subsequent training. This will benefit in archiving a better generalization and more stable feature high-level feature abstractions avoiding the influence of specific categories. The decoding block and the encoding block are almost completely symmetrical, except that the downsampling operation is replaced by an upsampling of the feature map. In the decoder network, the decoder layer fuse the feature map of corresponding encoder layer to assemble a more precise output based on this information. Thus, the underlying features of the encoder block can be more easily transmitted to the decoder and hence retaining more accurate information of object boundary and edges.

Feature-Sensitive Block

Inspired by the mechanism of human visual co-saliency, high-level semantic guidance as well as inter-image interaction at semantic level are important for co-saliency detection. This module aims to optimize the within image co-saliency task in a simple data-driven manner, thereby avoiding complex fusion strategies, improving the speed and making training simple and effective.

The structure is composed of three trainable 3×3 convolution layers. Our goal is to learn a mapping to make it sensitive to similar feature regions, such that:

$$R = F_{sensitive}(H, \theta), \quad (2)$$

where H is the semantic feature retained after feature extraction by encoder block, $F_{sensitive}$ is a mapping function

that takes the feature H as input, and outputs the mapped features into the decoder block by learning a set of hidden layers parameters θ .

We try to use the regional feature mapping network added in the training phase to supervise the Feature-Sensitive module and make it sensitive to common saliency object regions. The high-level semantic information are passed to guide learning of the decoder network, thereby achieving better saliency segmentation results.

Regional Feature Mapping Block

Considering two similar salient target object regions A and B (in the form of rectangular bounding boxes) in the image X , corresponding to the regions i and j in feature map H produced by the encoder block, is mapped to R (as marked in orange in Figure 2) through the Feature-Sensitive block R_i and R_j , respectively, then the RFM network transforms the region features in the R into corresponding feature vectors, such as:

$$V_i = F_{RFM}(R_i, \theta) \quad (3)$$

where F_{RFM} is a mapping function that takes the region feature map R_i as input, and outputs the corresponding fixed length feature vector V_i by learning a set of hidden layers parameters θ .

Therefore, the optimization objective of the RFM module is to minimize the Euclidean distance between any two similar salient objects feature vectors. But there are two challenges: the first one is how to map feature regions R_i and R_j of different scales to the same length vector, and the second one is that it is difficult for two identical objects to show exactly the same feature representation under the influence of different scales or other factors, such as the shooting angle and illumination. Therefore, it is difficult to measure the characteristic representation of two identical objects by Euclidean distance.

For the first problem, inspired by previous work (He *et al.* 2015; Ren *et al.* 2015; He *et al.* 2017), we use RoIAlign (He *et al.* 2017) to map regional features of different sizes to feature vectors of the same length, which is more accurate on pixel-align task compared with ROI Pool (Ren *et al.* 2015). The feature regions of different scales are subdivided into spatial ROI bins, eg., 7×7 bins, use bilinear interpolation to compute the exact values of the input features at four regularly sampled locations in each ROI bin, and aggregate the results in terms of max or average. However, due to this structure, the resulting feature vector will introduce more noise. Hence, we try to construct a special feature space, so that the features of similar salient object regions have the property of clustering. Specifically, the Euclidean distance of the feature vector corresponding to the similar object region is smaller than that corresponding to the dissimilar object region.

As shown in Figure 3, we select three different saliency proposals (in the form of rectangular bounding boxes) anchor region (A), positive region (B) and negative region (C) in the image I . The regions of A and B include a same salient classes. The regions of C includes a different salient region or a non-saliency object region.

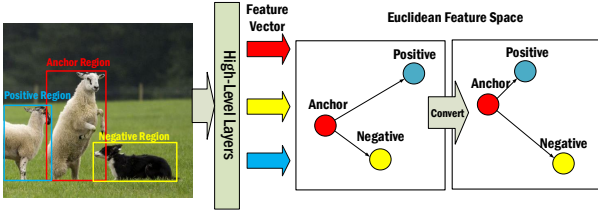


Figure 3: An illustration of the Euclidean Feature Space that high-level layers are mapped into. The positive pair consist of an anchor region and a positive region, which include two similar salient target object regions. The negative pair consist of an anchor region and a negative region. The feature vectors mapping by corresponding saliency regions in Euclidean Feature Space satisfy the clustering relationship during the training phase.

The feature vector corresponding to this triplet regions V_A, V_B, V_C should satisfy the following relationship in this feature space, such as:

$$\|V_A - V_B\|_2^2 < \|V_C - V_A\|_2^2, \quad (4)$$

Training

1) Sample Selection Strategy. A good sample selection strategy of positive and negative sample is necessary to get more robust feature space and avoid overfitting due to insufficient sample selection.

In the selection of triplet sample, the positive sample pair needs to be augmented. The positive pair is screened by generating jaccard overlap between the sample regions and the ground truth boxes. Specifically, in training phase, the selection of a positive pair must satisfy that each generated region contains only one salient object and match boxes to ground truth with Jaccard overlap higher than a threshold (0.5). It should be noted that the two generated sample regions can select the same salient target. As to negative sample, it can be the dissimilar saliency proposal with Jaccard overlap lower than a threshold (0.1) or the background regions.

We tried to generate positive and negative samples using an offline sample selection strategy and an online sample selection strategy. Offline strategy is to use ground-truth boxes to add random scaling and offset within a certain range, thereby satisfying the above sample generation conditions. The length-width ratio of the generated region ranges from 0.5 to 2, and the area of the generated region ranges from 128^2 to 512^2 . 32 positive samples and 96 negative samples are generated, and 128 triplets of training are randomly selected.

The other is to generate training samples online. In this strategy, we hope to find more difficult positive and negative samples to satisfy the generation conditions. In order to achieve online triplet mining, we need to evaluate the selected sample regions. We use the idea of online hard example mining (Shrivastava *et al.* 2016), which is designed to improve the accuracy of Fast RCNN. Specifically, we added Region Proposal Network(RPN) during the training process.

In our model, RPN is considered a sample region generator and evaluates the ease of the sample regions by its loss during training process. We selected the hard examples by sorting regions by training loss and use standard non-maximum suppression (NMS) to suppress only highly overlapping regions. We finally screen the hard positive and hard negative samples that satisfy the generation conditions to form a triple samples.

The experiment result shows this online strategy is better than the offline strategy with random scaling and offset, as shown in Table 1.

2) Loss Function. As shown in Figure 2, our network has three outputs during the training phase. The total loss function is a weighted sum of these three parts:

$$L_{total} = \alpha L_{decoder} + \beta L_{RPN} + \gamma L_{RFM}, \quad (5)$$

where α, β, γ are all set to 1.

The decoder block outputs the corresponding saliency map (Zou *et al.* 2019). The loss function of decoder part is computed by a pixel-wise cross-entropy loss with sigmoid between predicted saliency map P and the ground truth Y :

$$L_{decoder} = -\frac{1}{N} \sum_{i=1}^N [Y_i * \log(P_i) + (1 - Y_i) * \log(1 - P_i)] \quad (6)$$

where (P_i, Y_i) denotes the pixel values corresponding to the predicted saliency map and the ground truth.

For training RPN network, we select 9 anchor boxes with 3 scales with box areas of $(128^2, 256^2, 512^2)$ and 3 aspect ratios of (1:1, 1:2, 2:1). We select each ground truth box to the anchor box with the best Jaccard overlap as positive sample and select all anchors to any ground truth with Jaccard overlap higher than a threshold (0.5) as positive augmentation strategies. The label t is 1 if the anchor is positive, and is 0 if the anchor is negative. The loss function is similar to Faster R-CNN (Ren *et al.* 2015). We regress to anchor offsets for the center point (x, y) , length for width (w) and height (h) and the confidence of saliency object (c) . The loss function is a weighted sum of the localization part and the confidence confidence part:

$$L_{RPN} = \frac{1}{N} (L_{conf}(t, c) + \alpha L_{loc}(t, l, g)), \quad (7)$$

where N is the number of matched anchor boxes. The weight term α is set to 1 by cross validation. (l, g) contains the predicted box information including (x, y, w, h) and corresponding labels (g) . The localization loss is the Smooth L1 loss (Girshick 2015). Let d be the corresponding anchor box information for g , then we have

$$L_{loc}(p, l, g) = \sum_{i \in Pos} smooth_{L1}(l_i - \hat{g}_i), \quad (8)$$

$$\hat{g}_i^x = (g_i^x - d_i^x) / d_i^w,$$

$$\hat{g}_i^y = (g_i^y - d_i^y) / d_i^h,$$

$$\hat{g}_i^w = \log\left(\frac{g_i^w}{d_i^w}\right),$$



Figure 4: Sample images in our dataset. The new dataset contains more salient object instances, and some images are disturbed by other single salient objects (as in the bottom row).

$$\hat{g}_i^h = \log\left(\frac{g_i^h}{d_i^h}\right),$$

where \hat{g}_i is the anchor offsets between the ground-truth box and the corresponding anchor box.

For training RFM network, we use a weighted sum of triplet sample: *anchor(a)*, *positive(p)*, and *negative(n)*. The weight is calculated by

$$\beta_i = I(\text{anchor}, gt) * I(\text{positive}, gt), \quad (9)$$

where $I(\text{anchor}, gt)$ is the Jaccard overlap between the anchor box and the corresponding ground-truth box, and $I(\text{positive}, gt)$ is the Jaccard overlap between the positive box and the corresponding ground-truth box.

For some distance on the embedding space d , the loss of a triplet is defined as:

$$L_{RFM} = \max(d(V^a, V^p) - d(V^a, V^n) + \text{margin}, 0), \quad (10)$$

where V^a, V^p, V^n are the corresponding feature vectors to regions in the triplet samples, and *margin* is a margin that is enforced between positive and negative pairs. We minimize this loss, which pushes $d(V^a, V^p)$ to 0 and $d(V^a, V^n)$ to be greater than $d(V^a, V^p) + \text{margin}$. As for easy examples, the loss becomes zero.

Experiments

Datasets and Evaluation Metrics

The general standard dataset, such as iCoseg (Batra *et al.* 2010), MSRA (Liu *et al.* 2011) and HKU-IS (Li and Yu 2015), are all collected for within-image saliency detection or cross-image co-saliency detection methods. These datasets generally include just one saliency object or multiple objects with different classes. The SDCS dataset (Yu *et al.* 2018) is targeted for within-image co-saliency detection, however it just includes two to three co-salient objects in a single image. Hence, we created a larger targeted datasets with instance-level annotations. The dataset contains 2,019 natural images, over 300 daily necessities and 7,000 salient object instances.¹

¹Codes and data are available at <https://github.com/qinnzou/co-saliency-detection>

As shown in Figure 4, each image contains one class of two or more co-salient objects (with 3.52 objects in one image in average), and some images are disturbed by other single salient objects (like the second line in the picture), making the dataset more challenging. Each image contains at least two or more identical salient objects. Unlike other standard salient datasets, each object has its corresponding position labeling and contour labeling. The image size ranges from 450x256 to 808x1078 pixels.

In the experiments, we use four metrics to evaluate the performance by compute pixel-wise error between prediction saliency map and the mask of ground truth, which is mean absolute error (MAE), the Precision and Recall (PR) (Borji *et al.* 2015), and F-measure using adaptive thresholds (Achanta *et al.* 2009; Li and Yu 2016).

Implementation Details

In this paper, the weights of the 16-layer VGG pre-trained on ImageNet are used to initialize the encoder block and are fixed. In the model training, one image is input each time. To fully train the network, various data-augmentation operations are applied before the image input, including multi-scale scaling, random object clipping, random occlusion and so on. The experimental results in Table 1 has shown that data enhancement is very effective in reducing the over-fitting of triplet loss and improving the generalization ability of the model. We choose SGD as the optimizer in our experiment, and the learning rate and the weight decay are set to 1e-5 and 0.0001, respectively. Finally, the learning rate decreases to 1e-6 after 30,000 training iterations. It requires about 80,000 training iterations for convergence. We train the model on two NVIDIA GTX 1080Ti 11G GPUs and do the test using a single GPU. The running speed of the test is 28fps.

Model Analysis

In order to better analyze the role of each module, we conduct an ablation study by using a large number of horizontal comparison experiments. The results are shown in Table 1. From Table 1 we can see that, in the right part, the first column corresponds to the results using only the encoding and decoding network of the U-net structure, which achieves an accuracy of 82.4%, the lowest among all results. It indicates that only using a top-down strategy with only the masks as guidance cannot fully train the network to identify within-image co-saliency.

We can also see that, the accuracy of U-net improves 0.8% when training it with data augmentation, which is not a significant improvement. However, when adding the RFM layer in the training, both online and offline, the performance of co-saliency detection has a boosted improvement. It is because the RFM provides a bottom-up way to guide the network training and make it sensitive to co-salient regions.

Meanwhile, it can be seen that the results of the online version RFM are better than those of the offline version, which validates the effectiveness of the proposed online training sample selection strategy. Specifically, we speculate that there may be two reasons. First, the introduction of

Table 1: An ablation analysis of various design choices for the proposed method

The proposed method	With / Without						
Data augmentation	✓		✓	✓	✓	✓	✓
Feature-Sensitive block		✓	✓		✓	✓	✓
Offline training (RFM)				✓	✓		
Online training (RFM)							✓
F-measure (%)	82.4	83.2	82.3	83.6	88.1	89.2	90.4

Table 2: Results obtained by different methods on the two datasets

Method	Our Dataset				SDCS Dataset			
	F-Measure	Recall	Precision	MAE	F-Measure	Recall	Precision	MAE
FT (Achanta <i>et al.</i> 2009)	0.536	0.640	0.461	0.258	0.58	0.530	0.6	0.244
CWS (Fu <i>et al.</i> 2013)	0.707	0.764	0.658	0.166	0.767	0.7	0.79	0.165
U-Net (Ronneberger <i>et al.</i> 2015)	0.824	0.805	0.846	0.096	0.856	0.762	0.889	0.107
RFCN (Wang <i>et al.</i> 2016)	0.852	0.858	0.847	0.083	0.883	0.848	0.895	0.083
PiCANet (Liu <i>et al.</i> 2018)	0.856	0.883	0.83	0.086	0.854	0.841	0.869	0.088
DCL (Li and Yu 2016)	0.887	0.860	0.916	0.059	0.888	0.844	0.902	0.059
LFM (Yu <i>et al.</i> 2018)	0.893	0.881	0.907	0.051	0.903	0.85	0.912	0.050
Ours (offline)	0.892	0.870	0.917	0.050	0.907	0.855	0.924	0.048
Ours (online)	0.904	0.917	0.892	0.047	0.911	0.865	0.925	0.044

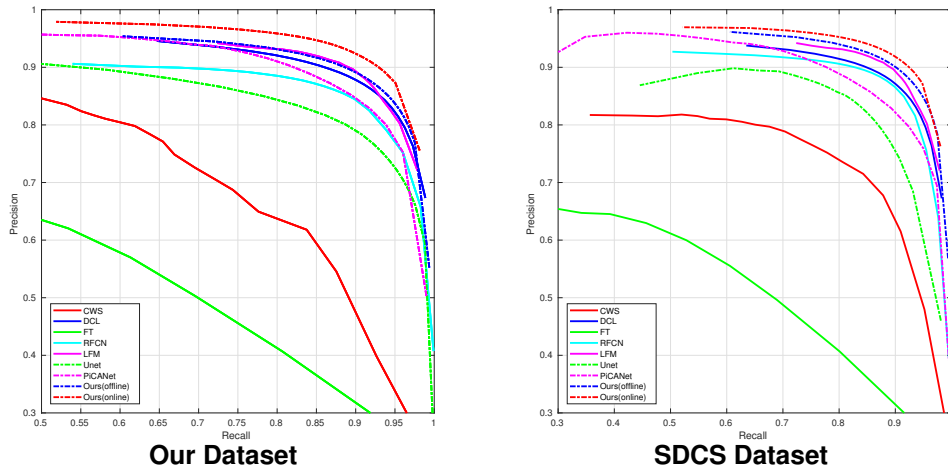


Figure 5: Precision-Recall curves obtained by the proposed method and the state-of-the-art methods on two datasets.

additional supervisory signals enhances the supervisory effect on the Feature-Sensitive layer. Second, the feature vectors generated by the sample region recommended by the RPN network introduce less noise than those generated by the randomly generated sample region. This helps to better learn the characteristics of the feature space.

In addition, comparing the results in the last second and the last third columns, we can see that data augmentation brings a significant improvement on the performance. This is because the data augmentation can better train the RFM module.

Comparison with State-of-the-Art Methods

We compare the results of our method with other representative saliency detectors. Among them, DCL (Li and Yu 2016), RFCN (Wang *et al.* 2016), LFM (Yu *et al.* 2018), PiCANet (Liu *et al.* 2018), U-net (Simonyan and Zisserman 2014) are

deep learning-based methods, CWS (Fu *et al.* 2013) and FT (Achanta *et al.* 2009) are traditional saliency detection methods.

In order to make a fair comparison, we train the comparison methods on our dataset by using the recommended parameter settings. We compute the average performance for these models with respect to F-measure, MAE, Recall and Precision. The results are shown in Table 2.

In the experiment results, deep learning-based methods obtain better saliency results than traditional methods. The baseline model (U-net) has worse saliency results than other deep learning based networks. Our method, whose evaluation part is based on skip-layer connection structure of U-net, achieves better average recall and better average precision than other saliency methods DCL, RFCN, PiCANet. It is because that these saliency detection methods cannot judge co-saliency objects very well even though trained by

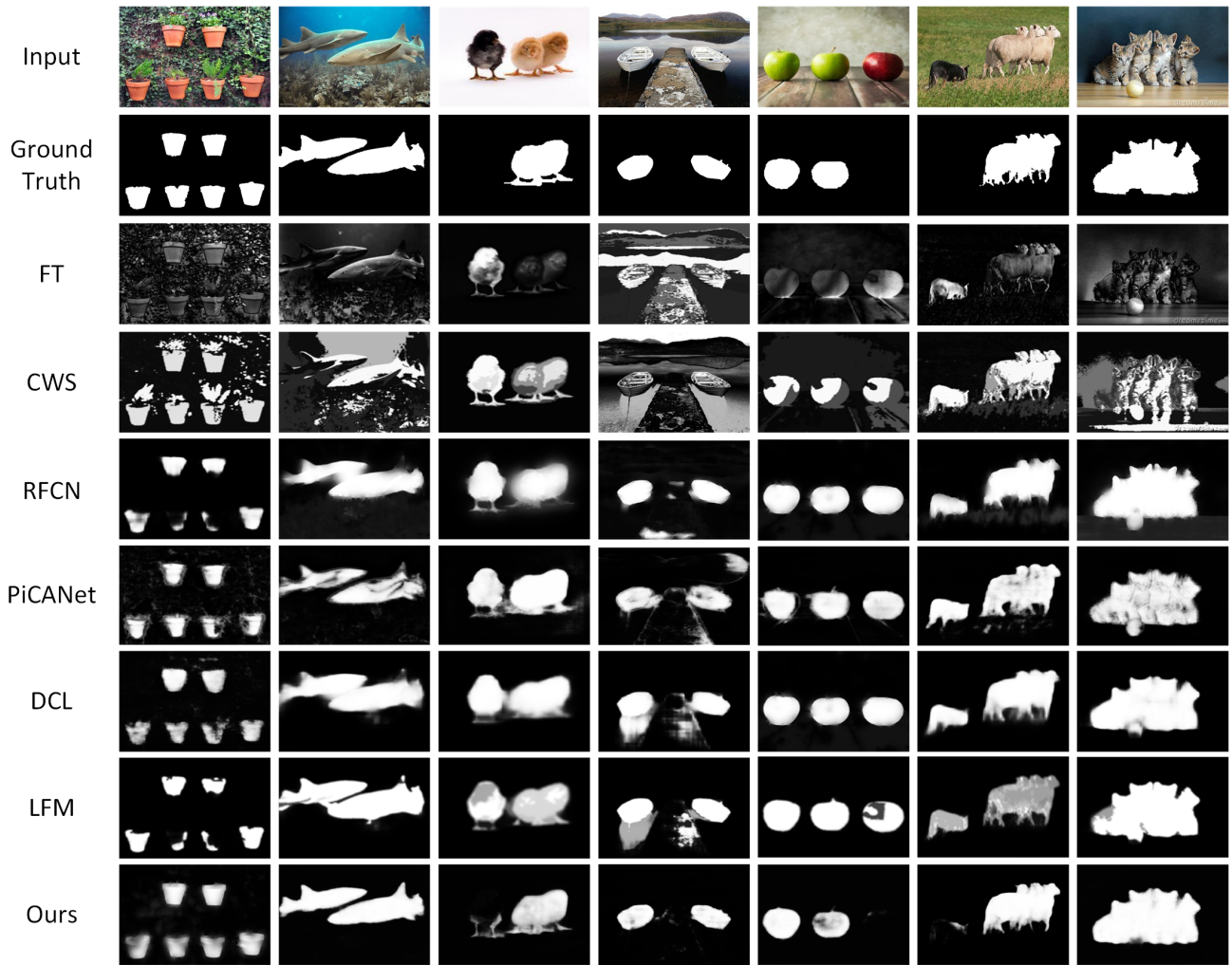


Figure 6: Visual comparison for the performance of different methods.

the correct co-saliency masks, which can also be seen in the visual comparison results in Figure 6. And our method as an end-to-end framework, has a faster speed than the LFM and has a higher average precision.

For quantitative comparison, the Precision-Recall curves obtained SDCS dataset are plotted in Figure 5. It can be observed that, the proposed method has the highest performance. And the online version of the proposed method, i.e., using online training strategy, is better than the offline version, which are consistent with the results in Table 2.

Visual comparison

We also visually compare the results obtained by our method and five comparison methods on several sample images, which are shown in Figure 6. We select some easy images and hard images that include other disturbed saliency objects. From this results, we can find that the U-net structure can save many saliency details which are helpful to produce more accurate edges in the segmentation task. Compared with other methods in hard images, general saliency detec-

tors based on deep learning cannot judge co-saliency objects using only masks as the supervision information. We train the high-level hidden layers to learn the mapping of the pure saliency sensitivity to co-saliency objects sensitivity, which leads to better results.

Conclusion

In this paper, a novel end-to-end network for within-image co-saliency detection was proposed. It combined the top-down and bottom-up strategies. Specifically, an encoder-decoder net was employed for co-saliency map prediction in a top-down manner, and a region proposal network (RPN) and a regional feature mapping network (RFM) were used to guide the model to be sensitive to co-salient regions, in a bottom-up manner. An online training sample selection algorithm was presented to enhance the performance of the proposed network. Experimental results on two targeted datasets showed that the proposed method achieved the state-of-the-art accuracy while running in a speed of 28fps.

References

- Radhakrishna Achanta, Sheila Hemami, Francisco Estrada, and Sabine Susstrunk. Frequency-tuned salient region detection. In *IEEE Conference on Computer Vision and Pattern Recognition*, 2009.
- Dhruv Batra, Adarsh Kowdle, Devi Parikh, Jiebo Luo, and Tsuhan Chen. icoseg: Interactive co-segmentation with intelligent scribble guidance. In *IEEE Conference on Computer Vision and Pattern Recognition*, pages 3169–3176, 2010.
- Sean Bell and Kavita Bala. Learning visual similarity for product design with convolutional neural networks. *ACM Transactions on Graphics*, 34(4):98, 2015.
- Ali Borji, Ming-Ming Cheng, Huaizu Jiang, and Jia Li. Salient object detection: A benchmark. *IEEE transactions on image processing*, 24(12):5706–5722, 2015.
- Xiaochun Cao, Zhiqiang Tao, Bao Zhang, Huazhu Fu, and Wei Feng. Self-adaptively weighted co-saliency detection via rank constraint. *IEEE Transactions on Image Processing*, 23(9):4175–4186, 2014.
- Ming-Ming Cheng, Niloy J Mitra, Xiaolei Huang, Philip HS Torr, and Shi-Min Hu. Global contrast based salient region detection. *IEEE Transactions on Pattern Analysis and Machine Intelligence*, 37(3):569–582, 2014.
- Jia Deng, Wei Dong, Richard Socher, Li-Jia Li, Kai Li, and Li Fei-Fei. Imagenet: A large-scale hierarchical image database. In *IEEE Conference on Computer Vision and Pattern Recognition*, 2009.
- Huazhu Fu, Xiaochun Cao, and Zhuowen Tu. Cluster-based co-saliency detection. *IEEE Transactions on Image Processing*, 22(10):3766–3778, 2013.
- Ross Girshick. Fast r-cnn. In *IEEE International Conference on Computer Vision*, pages 1440–1448, 2015.
- Stas Goferman, Lih Zelnik-Manor, and Ayellet Tal. Context-aware saliency detection. *IEEE transactions on pattern analysis and machine intelligence*, 34(10):1915–1926, 2011.
- Kaiming He, Xiangyu Zhang, Shaoqing Ren, and Jian Sun. Spatial pyramid pooling in deep convolutional networks for visual recognition. *IEEE transactions on pattern analysis and machine intelligence*, 37(9):1904–1916, 2015.
- Kaiming He, Georgia Gkioxari, Piotr Dollár, and Ross Girshick. Mask r-cnn. In *IEEE international conference on computer vision*, pages 2961–2969, 2017.
- Xiaodi Hou and Liqing Zhang. Saliency detection: A spectral residual approach. In *IEEE Conference on Computer Vision and Pattern Recognition*, pages 1–8, 2007.
- Rui Huang, Wei Feng, and Jizhou Sun. Color feature reinforcement for cosaliency detection without single saliency residuals. *IEEE Signal Processing Letters*, 24(5):569–573, 2017.
- Guanbin Li and Yizhou Yu. Visual saliency based on multi-scale deep features. In *IEEE Conference on Computer Vision and Pattern Recognition*, pages 5455–5463, 2015.
- Guanbin Li and Yizhou Yu. Deep contrast learning for salient object detection. In *IEEE Conference on Computer Vision and Pattern Recognition*, pages 478–487, 2016.
- Tie Liu, Zejian Yuan, Jian Sun, Jingdong Wang, Nanning Zheng, Xiaoou Tang, and Heung-Yeung Shum. Learning to detect a salient object. *IEEE Transactions on Pattern Analysis and Machine Intelligence*, 33(2):353–367, 2011.
- Nian Liu, Junwei Han, and Ming-Hsuan Yang. Picanet: Learning pixel-wise contextual attention for saliency detection. In *IEEE Conference on Computer Vision and Pattern Recognition*, pages 3089–3098, 2018.
- Shaoqing Ren, Kaiming He, Ross Girshick, and Jian Sun. Faster r-cnn: Towards real-time object detection with region proposal networks. In *Advances in neural information processing systems*, pages 91–99, 2015.
- Olaf Ronneberger, Philipp Fischer, and Thomas Brox. U-net: Convolutional networks for biomedical image segmentation. In *International Conference on Medical image computing and computer-assisted intervention*, pages 234–241, 2015.
- Florian Schroff, Dmitry Kalenichenko, and James Philbin. Facenet: A unified embedding for face recognition and clustering. In *IEEE conference on computer vision and pattern recognition*, pages 815–823, 2015.
- Abhinav Shrivastava, Abhinav Gupta, and Ross Girshick. Training region-based object detectors with online hard example mining. In *IEEE conference on computer vision and pattern recognition*, pages 761–769, 2016.
- Karen Simonyan and Andrew Zisserman. Very deep convolutional networks for large-scale image recognition. *arXiv preprint arXiv:1409.1556*, 2014.
- Linzhao Wang, Lijun Wang, Huchuan Lu, Pingping Zhang, and Xiang Ruan. Saliency detection with recurrent fully convolutional networks. In *European conference on computer vision*, pages 825–841, 2016.
- Wenguan Wang, Jianbing Shen, and Ling Shao. Video salient object detection via fully convolutional networks. *IEEE Transactions on Image Processing*, 27(1):38–49, 2018.
- Lina Wei, Shanshan Zhao, Omar El Farouk Bourahla, Xi Li, and Fei Wu. Group-wise deep co-saliency detection. *arXiv preprint arXiv:1707.07381*, 2017.
- Hongkai Yu, Kang Zheng, Jianwu Fang, Hao Guo, Wei Feng, and Song Wang. Co-saliency detection within a single image. In *AAAI*, 2018.
- Ting Zhao and Xiangqian Wu. Pyramid feature attention network for saliency detection. In *IEEE Conference on Computer Vision and Pattern Recognition*, pages 3085–3094, 2019.
- C Lawrence Zitnick and Piotr Dollár. Edge boxes: Locating object proposals from edges. In *European conference on computer vision*, pages 391–405, 2014.
- Qin Zou, Zheng Zhang, Qingquan Li, Xianbiao Qi, Qian Wang, and Song Wang. Deepcrack: Learning hierarchical convolutional features for crack detection. *IEEE Transactions on Image Processing*, 28(3):1498–1512, 2019.